

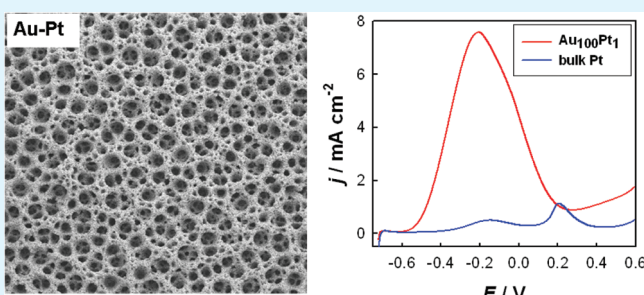
# Preparation of AuPt Alloy Foam Films and Their Superior Electrocatalytic Activity for the Oxidation of Formic Acid

Jun Liu, Ling Cao, Wei Huang, and Zelin Li\*

Key Laboratory of Chemical Biology and Traditional Chinese Medicine Research (Ministry of Education of China), College of Chemistry and Chemical Engineering, Hunan Normal University, Changsha 410081, China

 Supporting Information

**ABSTRACT:** AuPt alloy films with three-dimensional (3D) hierarchical pores consisting of interconnected dendrite walls were successfully fabricated by a strategy of cathodic codeposition utilizing the hydrogen bubble dynamic template. The foam films were characterized by scanning electron microscopy (SEM), X-ray diffraction (XRD), and X-ray photoelectron spectroscopy (XPS). Due to the special porous structure, the electronic property, and the assembly effect, the AuPt alloy foam films show superior electrocatalytic activity toward the electrooxidation of formic acid in acidic solution, and the prepared 3D porous AuPt alloy films also show high activity and long stability for the electrocatalytic oxidation of methanol, where synergistic effect plays an important role in addition to the electronic effect and assembly effect. These findings provide more insights into the AuPt bimetallic nanomaterials for electrocatalytic applications.



**KEYWORDS:** foam film, AuPt alloy, dendrite, electrodeposition, hydrogen bubble template, formic acid, methanol, electrocatalysis

## 1. INTRODUCTION

Alloyed nanomaterials in which the d-band vacancies of a Group VIII metal are progressively filled by the addition of a Group IB metal have attracted particular interest from the electronic viewpoint.<sup>1–8</sup> Large efforts are being directed toward the synthesis of these alloy nanomaterials for the application of fuel cells because they often exhibit higher electrocatalytic activities than monometallic nanocatalysts toward the oxidation of small organic molecules.<sup>9–15</sup> The catalytic properties of bimetallic catalysts depend on their surface structure and composition. Accordingly, rationally designed bimetallic nanocatalysts with controlled morphology and component may show attracting properties.

Among the various noble bimetallic nanomaterials, the promotional effects of platinum on/in gold have been extensively investigated by many groups.<sup>11,16–30</sup> Alloying Pt with Au is expected to improve the catalytic activity of Pt by the electronic effect,<sup>2,14,26,31</sup> ensemble effect,<sup>20</sup> and/or synergistic effect.<sup>3,21,23,24,27</sup> The electronic effect is a result of the d-band center shift of Pt in the AuPt alloys. The ensemble effect is defined in terms of the arrangement of surface atoms of a particular pattern required for being active to a given kind of reactant molecules. The synergistic effect means that Pt and Au in the alloys have perspective functions and act cooperatively in the electrocatalysis. These are the main theoretical descriptions currently employed for the bimetallic electrocatalysts. Moreover, nanostructures and surface morphologies of AuPt bimetallic materials also play important roles in catalysis. Nanocrystals,<sup>25</sup> nanorods,<sup>32</sup> nanowires,<sup>33</sup> and thin films

of nanonetworks<sup>34</sup> are the examples of nanomaterials usually employed.

Three-dimensional (3D) porous materials with hierarchical structures allow not only fast mass transport of ion/gas through the electrolyte/electrode interface (due to short diffusion length) but also rapid electrochemical reactions (due to considerable high active surface area). In the past two decades, great efforts have been made in controllably fabricating 3D porous nanostructures. Among various synthetic strategies of 3D porous structures, templating<sup>35–39</sup> and dealloying<sup>40–42</sup> are the two most popular methods. Although hydrogen bubble dynamic templates have been developed recently in electrodeposition of self-supported 3D foam films like Au,<sup>43,44</sup> Ag,<sup>45</sup> Sn,<sup>46</sup> Cu,<sup>46,47</sup> and CuSn,<sup>48</sup> little attention has been devoted up to date to prepare alloy foam films of noble metals by this simple, fast, and green route. Moreover, the relationship of structure and component of AuPt alloy foam films with their electrocatalytic property still need to be explored.

In this study, we prepare AuPt alloy foam films by cathodic codeposition utilizing the hydrogen bubble dynamic templates. The component of the foam films was controlled by adjusting the molar ratio of the two metal precursors in the feeding solutions. The electrocatalytic activities of such unique AuPt alloy foam films toward the oxidation of formic acid and methanol have been investigated for the first time.

**Received:** June 17, 2011

**Accepted:** August 12, 2011

**Published:** August 12, 2011

## 2. EXPERIMENTAL SECTION

**2.1. Reagents.** HAuCl<sub>4</sub>·4H<sub>2</sub>O and H<sub>2</sub>PtCl<sub>6</sub>·6H<sub>2</sub>O were obtained from Sinopharm Chemical Reagent Co. Ltd. (Shanghai, China). Sulfuric acid, formic acid, and methanol were purchased from the Factory of Hunan Normal University. All the chemicals were of analytical grade and were used as received. Milli-Q water with a resistivity of greater than 18.3 MΩ·cm was used in the preparation of aqueous solutions.

**2.2. Electrodeposition of 3D Porous AuPt Films.** Electrochemical experiments were performed on a CHI 660C electrochemical workstation (Chenhua Instruments, Shanghai, China). A gold disk (1 mm diameter, purity 99.99%), a platinum foil (geometric area 1 cm<sup>2</sup>), and a saturated mercurous sulfate electrode (SMSE) were employed as the working, counter, and reference electrodes, respectively. Prior to use, the working electrode was polished with 2000 grit carbimet paper, followed by rinsing in Millipore water under ultrasonic waves. Then, the electrode was electrochemically pretreated by cycling the potential between -0.7 and +1.1 V in 0.5 M H<sub>2</sub>SO<sub>4</sub> at a scan rate of 100 mV s<sup>-1</sup> until a stable voltammogram was obtained. We first optimized the electrodeposition conditions of gold foams at room temperature (~25 °C) by varying the deposition time (10 s, 100 s, 300 s, 500 s), deposition potential (-1.5 V, -3 V, -4 V, -5 V), sulfuric acid concentration (0.5 M, 2 M, 5 M, 10 M), and gold concentration (0.4 mM, 2 mM, 5 mM, 10 mM). These results are provided in Figure S1–S4 in the Supporting Information. Then, the electrodeposition of AuPt foams were carried out under the effective conditions to create porous Au foam (-4 V, 300 s). We did so because the content of Pt in the AuPt foams is low to save Pt, and we denoted the deposited foam films as Au<sub>100</sub>Pt<sub>1</sub>, Au<sub>100</sub>Pt<sub>6</sub>, and Au<sub>100</sub>Pt<sub>8</sub>, respectively, according to the mole ratio of HAuCl<sub>4</sub>/H<sub>2</sub>PtCl<sub>6</sub> in the feeding solutions: 2 mM HAuCl<sub>4</sub> + x mM H<sub>2</sub>PtCl<sub>6</sub> + 2 M H<sub>2</sub>SO<sub>4</sub> (x = 0.02, 0.12, and 0.16).

**2.3. Characterizations of the Deposited Foam Films.** The morphology images of the electrodeposited foam films were taken with a JEOL JSM-6360 scanning electron microscope (SEM) operating at 25 kV. X-ray diffraction (XRD) patterns were obtained with a Dmax Rapid IIR diffractometer using Cu K $\alpha$  (0.1542 nm) radiation, and the exposure time was 15 min. The surface composition and the electronic structure of the electrodeposited AuPt foam films were analyzed with an ESCA-Lab250 X-ray photoelectron spectroscopy (XPS).

**2.4. Electrooxidation of Formic Acid and Methanol.** The deposited AuPt alloy foam films and pure metal electrodes were first treated by cyclic voltammetry between -0.7 and 1.1 V at 100 mV s<sup>-1</sup> in 0.5 M H<sub>2</sub>SO<sub>4</sub> solution until a steady cyclic voltammogram (CV) was obtained. The current densities of AuPt alloy catalysts for methanol oxidation were normalized to the total electrochemical active surface areas (ECSAs), which were calculated using 386 μC cm<sup>-2</sup> and 210 μC cm<sup>-2</sup> for the reduction of Au oxide monolayer and for the hydrogen ad/desorption at Pt, respectively. Only the ECSAs of Pt in the AuPt foams were calculated using hydrogen ad/desorption peak for the oxidation of formic acid, considering that Au had no catalytic activity in this case.

The electrocatalytic activity toward the electrooxidation of formic acid and methanol was evaluated in solutions of 0.5 M H<sub>2</sub>SO<sub>4</sub> + 0.5 M HCOOH and 0.5 M NaOH + 0.5 M CH<sub>3</sub>OH, respectively, and the linear sweep voltammetry was recorded in the potential ranges between -0.72 and 0.75 V and between -1.42 and 0.4 V for the oxidation of formic acid and methanol, respectively. The current density-time (*j*-*t*) curves were measured at a fixed potential for 2000 s.

**2.5. Poison Adsorption and Stripping.** The poison formation on the deposited electrodes under open circuit potential in 0.5 M formic acid solution was studied as described in ref 49. Briefly, the electrode was activated by cyclic voltammetry in 0.5 M H<sub>2</sub>SO<sub>4</sub> within the potential range of -0.7 to 1 V, rinsed with pure water, and put in contact with 0.5 M formic acid solution for 3 min. The electrode was then transferred

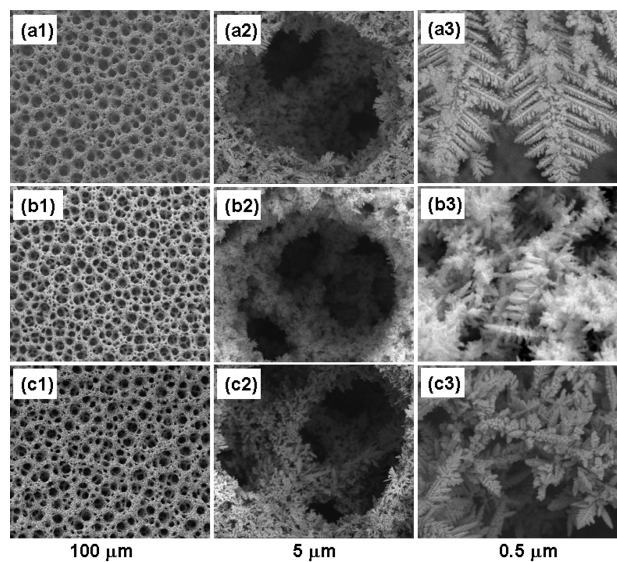


**Figure 1.** SEM images with different enlargement scales for the 3D porous alloy foams of (a1–a3) Au<sub>100</sub>Pt<sub>1</sub>, (b1–b3) Au<sub>100</sub>Pt<sub>6</sub>, and (c1–c3) Au<sub>100</sub>Pt<sub>8</sub>.

to deaerated Milli-Q water and rotated to clean the excess HCOOH from the surface of the electrode. Then, the electrodes were transferred back to the electrochemical cell containing 0.5 M H<sub>2</sub>SO<sub>4</sub> at -0.6 V vs SMSE. The adsorbed poison was stripped by scanning the potential positively within the range of -0.7 to 0.4 V starting at -0.6 V.

## 3. RESULTS AND DISCUSSION

**3.1. Characterizations of the Electrodeposited Foam Films.** The SEM images in Figure 1 show the porous structure of the AuPt foam films with different components by electrodeposition along with H<sub>2</sub> evolution at a constant potential of -4 V for 300 s. The porous structure of these forms looks similar to each other (column 1, 100 μm), resembling that of pure Au foam (Figure S1 in the Supporting Information). The pore size of the foam films increases from bottom to top up to about 30 μm due to the coalescence of hydrogen gas bubbles during evolution from the substrate. The pores are highly connected, and the walls are composed of dense dendrites (column 2, 5 μm). The AuPt alloy foams may have larger surface areas and more active sites. Further comparison by enlarging the image displays that their dendrites in the wall differ to some extent in size and shape (column 3, 0.5 μm), which may also make some differences in electrocatalysis.

XPS characterizations were carried out to get surface composition of the electrodeposited alloy foam films. Figure 2 presents the Pt 4f (panel a) and Au 4f (panel b) spectra from the 3D porous AuPt catalysts with different precursor atomic ratios. The binding energies (BEs) of the 4f signals for Pt<sup>0</sup> and Au<sup>0</sup> components in the deposited samples are summarized in Table 1. The BEs of Pt 4f<sub>7/2</sub> and Pt 4f<sub>5/2</sub> in the AuPt foam films were less than that of bulk Pt (Table 1)<sup>50</sup> and became lower while the Pt content decreased. In contrary, the BEs of Au 4f<sub>7/2</sub> and Au 4f<sub>5/2</sub> got higher with the decrease of Au content in the AuPt foam films. These BE changes suggest that Au and Pt in the foams were atomically mixed with no phase separation, and they can be attributed to the electron effect and the geometric effect by the alloying. Note that Au and Pt have filled (d<sup>10</sup>) and unfilled (d<sup>9</sup>)

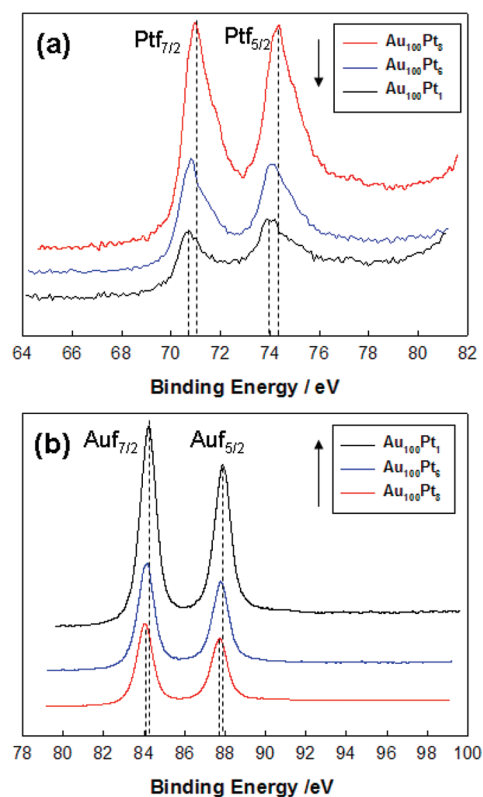


**Figure 2.** XPS spectra of 3D porous AuPt samples. (a) Pt 4f peaks; (b) Au 4f peaks.

**Table 1. Binding Energies and Relative Contents of Platinum and Gold in the Foam Films**

sample	BE				atom %		
	Ptf <sub>7/2</sub> , eV	Ptf <sub>5/2</sub> , eV	Auf <sub>7/2</sub> , eV	Auf <sub>5/2</sub> , eV	Pt	Au	Pt <sup>a</sup>
Au <sub>100</sub> Pt <sub>1</sub>	70.66	73.91	84.02	87.72	2.14	97.86	0.99%
Au <sub>100</sub> Pt <sub>6</sub>	70.78	74.09	84.09	87.77	8.36	91.64	5.66%
Au <sub>100</sub> Pt <sub>8</sub>	70.93	74.36	84.19	87.86	9.32	90.68	7.40%
SBE <sup>b</sup>	71.00	74.40	84.00	87.70			

<sup>a</sup> Pt in feeding solutions. <sup>b</sup> SBE: standard binding energy.<sup>50</sup>

d-orbitals, respectively, and the atomic radius of Au is larger than that of Pt. Bagus et al. demonstrated that both of the intra-atomic charge arrangement and the interatomic charge transfer (from Au to Pt here) could make contributions to the BE changes.<sup>51,52</sup> Similar BE shifts have also been observed previously for AuPt alloys,<sup>14,53</sup> for Pt alloys with other transition metals like Ag<sup>8</sup> and Ni,<sup>54</sup> and for Pt-TiO<sub>2</sub>.<sup>53</sup> However, opposite variation trend has been reported for the BEs of Pt and/or Au depending on different conditions, such as substrate,<sup>2</sup> composition,<sup>3,55</sup> and phase segregation.<sup>14</sup> Electronegativity difference<sup>3,55</sup> and strain effect<sup>14</sup> may also result in the BE shift. These facts indicate that subtle measures should be taken to control the electronic properties of alloy electrocatalysts.

The relative abundances at the surface of the AuPt foam films detected by XPS are also summarized in Table 1. The atomic percent of Pt in the samples of Au<sub>100</sub>Pt<sub>1</sub>, Au<sub>100</sub>Pt<sub>6</sub>, and Au<sub>100</sub>Pt<sub>8</sub> obtained from the XPS are somewhat higher than that in the feeding solutions. The enrichment of Pt on the surface of the

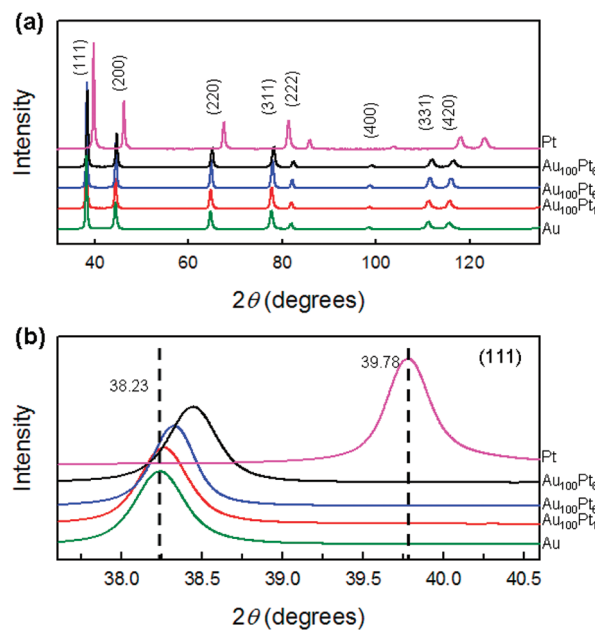


**Figure 3.** (a) XRD patterns and (b) comparison of (111) diffraction peaks for the prepared AuPt alloy foam films. The XRD patterns of pure metals of Au and Pt were also given for comparison.

porous structures might be due to the stronger hydrogen adsorption on Pt than on Au at -4 V.

In order to further determine the feature of bulk phase, the as-prepared foam films were characterized by XRD. Figure 3a shows the XRD patterns of the deposited foam films of AuPt alloy (Au<sub>100</sub>Pt<sub>1</sub>, Au<sub>100</sub>Pt<sub>6</sub>, and Au<sub>100</sub>Pt<sub>8</sub>) in comparison with pure Pt and Au. The peaks at 38.23°, 44.34°, 64.63°, 77.65°, 81.89°, 98.38°, 110.98°, 115.55°, and 135.91° are assigned to Au (111), (200), (220), (311), (222), (400), (331), (420), and (422), respectively, according to JCPDS 04-0784; and the peaks at 39.78°, 46.23°, 67.53°, 81.39°, 85.87°, 103.73°, 118.04°, and 123.14° are assigned to Pt(111), (200), (220), (311), (222), (400), (331), and (420), respectively, according to JCPDS 04-0802.

The XRD patterns in the range between 37.6° and 40.6° in Figure 3a are enlarged in Figure 3b. Careful comparisons show that the peaks of Au<sub>100</sub>Pt<sub>1</sub>, Au<sub>100</sub>Pt<sub>6</sub>, and Au<sub>100</sub>Pt<sub>8</sub> samples fall well between the (111) peaks of pure Au and Pt, suggesting that the AuPt porous films are, indeed, a single-phase alloy nanomaterial rather than a mixture of monometallic Au and Pt or a core–shell structure of Au and Pt. The refined d-space parameters of all samples are presented in Table S1 in the Supporting Information.

Theoretical calculations show that bimetallic AuPt nanoparticles are inclined to form core–shell or onion-like structures,<sup>56</sup> and AuPt alloys could be synthesized by reducing the particle size.<sup>57</sup> However, the preparation of AuPt alloy nanostructures is still complicated because of the different reduction kinetics of Au and Pt ions.<sup>58</sup> Depending on the preparation conditions, the bimetallic composition, and the supporting materials, bimetallic nanoparticles of Au and Pt have been demonstrated to exist in alloy, partial alloy, and/or separated phases.<sup>59</sup> There are also some unique measures to promote alloy formation between Au and Pt, such as by a transmetalation process using Cu seeds inside a dendrimer template<sup>60</sup> and by decomposing bimetallic molecular clusters.<sup>61</sup> In this paper, we obtained AuPt alloys by

coelectrodeposition at  $-4$  V under diffusion control by adjusting the precursors' ratio in bath.

**3.2. Electrocatalytic Activity of the Electrodeposited AuPt Foam Films for the Oxidation of Formic Acid.** The electrocatalytic activity of the deposited AuPt alloy foam catalysts toward the oxidation of formic acid was evaluated in  $0.5$  M  $\text{H}_2\text{SO}_4 + 0.5$  M  $\text{HCOOH}$  electrolyte solution. The ECSAs of the electrodeposited electrodes are given in Table 2, which were obtained from the CVs in Figure 4 by integrating the hydrogen desorption charge at Pt and the reduction charge of monolayer gold oxide in  $0.5$  M  $\text{H}_2\text{SO}_4$  (after correcting the double layer charge). An earlier report showed that slow dissolution of the Au counter electrode (anode) in  $1$  M  $\text{H}_2\text{SO}_4$  occurred.<sup>62</sup> However, no reduction peak of Pt oxide was observed for the pure Au foam film in Figure 4, which means that the influence from the dissolution of the Pt counter electrode could be negligible in

**Table 2. ECSAs of Foam Films of AuPt Alloys and Pure Au**

sample	$\text{Pt}_{\text{ECSA}}$ cm <sup>2</sup>	$\text{Au}_{\text{ECSA}}$ cm <sup>2</sup>
Au		10.88
$\text{Au}_{100}\text{Pt}_1$	0.68	13.61
$\text{Au}_{100}\text{Pt}_6$	3.47	14.80
$\text{Au}_{100}\text{Pt}_8$	3.82	13.73

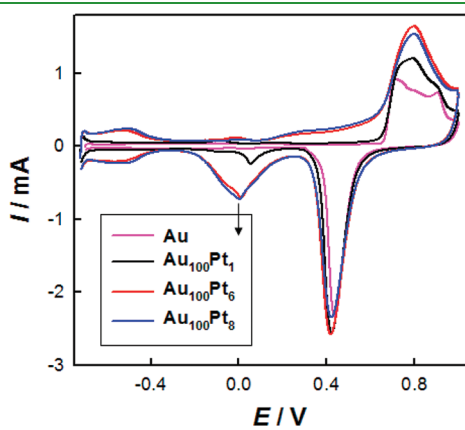


**Figure 4.** CVs of 3D porous AuPt alloy films and pure 3D porous Au film in  $0.5$  M  $\text{H}_2\text{SO}_4$  at  $50 \text{ mV s}^{-1}$ .

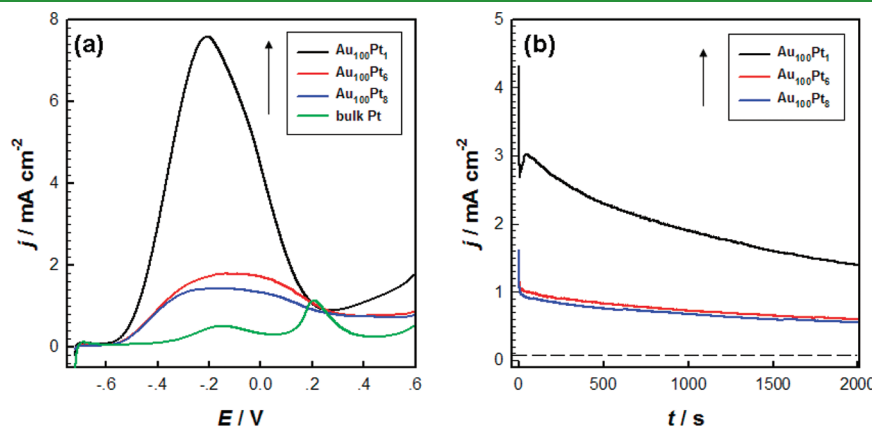
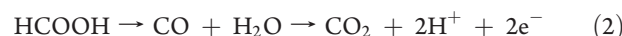


**Figure 5.** (a) Linear sweep voltammetry in  $0.5$  M  $\text{H}_2\text{SO}_4 + 0.5$  M  $\text{HCOOH}$  (the third cycle) at  $50 \text{ mV s}^{-1}$  and (b) chronoamperometric curves in  $0.5$  M  $\text{H}_2\text{SO}_4 + 0.5$  M  $\text{HCOOH}$  at  $-0.315$  V for the electrodes of deposited 3D porous AuPt alloy foam films and bulk Pt electrode. The dashed line shows the steady current density of commercial Etek-Pt/C<sup>28</sup> converted from the mass current density taking  $54.7 \text{ m}^2/\text{g}$  Pt as referenced in the Supporting Information.

such a short electrodeposition time ( $300$  s). The data in Table 2 reveal that the AuPt alloy foams possess larger surface area than the pure Au foam film, since Au was catalytically inactive toward the oxidation of formic acid under the experimental conditions performed here. Therefore, the measured current for formic acid oxidation was normalized by the ECSAs of Pt.

Figure 5a shows the positive scan curves for the electrooxidation of formic acid at the AuPt foam films. As we know, formic acid oxidation on Pt is considered as a model reaction in organic fuel electrocatalysis. This is because the oxidation of formic acid is a simple surface sensitive process that involves only two electrons. The reaction occurs through a dual path mechanism, summarized earlier by Capon and Parsons:<sup>63,64</sup>



The first peak on Pt in Figure 5a around  $-0.15$  V is related to the oxidation of  $\text{HCOOH}$  into  $\text{CO}_2$  via the active intermediate (path 1), while the second peak on Pt at  $0.21$  V represents the oxidation process via the poisonous  $\text{CO}_{\text{ads}}$  intermediate (path 2) generated from the dissociative adsorption of  $\text{HCOOH}$ . The adsorbed  $\text{CO}_{\text{ads}}$  can inhibit the catalytic oxidation of formic acid at the lower potential via path (1).<sup>63,64</sup> However, the electrodeposited AuPt foam films show dramatically enhanced electrocatalytic activity toward the oxidation of formic acid. The onset oxidative potential on them shifted negatively about  $200$  mV, and the first oxidation peaks related to the active intermediate became substantially higher. The peak current densities on the foam films of  $\text{Au}_{100}\text{Pt}_1$ ,  $\text{Au}_{100}\text{Pt}_6$ , and  $\text{Au}_{100}\text{Pt}_8$  were  $7.53$ ,  $1.74$ , and  $1.35 \text{ mA cm}^{-2}$ , respectively. A performance comparison toward the oxidation of formic acid has also been made between the electrodeposited AuPt alloy foam films and the commercial Etek-Pt/C as summarized in Table S2 in the Supporting Information. The results demonstrate that the AuPt alloy foam films prepared in this work have better catalytic activity than the commercial Etek-Pt/C. Meanwhile, the second oxidation peaks related to the poisonous  $\text{CO}_{\text{ads}}$  vanished on the alloy foam films. This enhanced catalytic activity can be explained with the ensemble effect.<sup>14</sup> It has been demonstrated that at least three

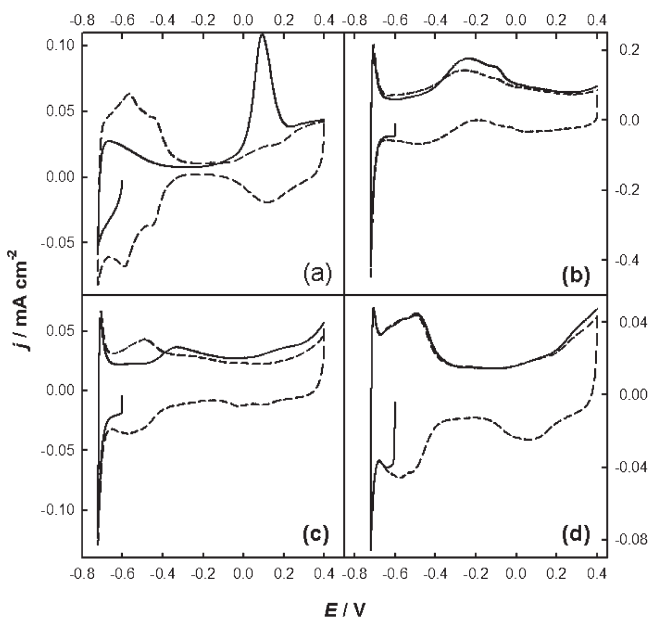


**Figure 6.** CVs in  $0.5\text{ M H}_2\text{SO}_4$  at  $50\text{ mV s}^{-1}$  for the poison stripping adsorbed from  $0.5\text{ M HCOOH}$  on (a) the pure Pt electrode and on the foam films of (b)  $\text{Au}_{100}\text{Pt}_1$ , (c)  $\text{Au}_{100}\text{Pt}_6$ , and (d)  $\text{Au}_{100}\text{Pt}_8$ . The full lines show the first positive sweeps while the dotted lines show the subsequent sweeps upon removal of the poisonous species.

neighboring Pt atoms were required for the dehydration path (formation of adsorbed CO) but one isolated Pt atom was enough for the dehydrogenation path in the formic acid electro-oxidation process.<sup>65</sup> Our results suggest that the Pt atoms in the AuPt foams were highly dispersed. The outstanding catalytic activity of sample  $\text{Au}_{100}\text{Pt}_1$  in comparison with  $\text{Au}_{100}\text{Pt}_6$  or  $\text{Au}_{100}\text{Pt}_8$  confirms that isolated single Pt sites favor the dehydrogenation path in formic acid electrooxidation.

On another hand, the electronic effect may also make contributions to the catalytic activity. In the AuPt alloy foam films, the d-band center of Pt shifts to a higher level<sup>27,31</sup> as evidenced by XPS in Figure 2 where the BEs of Pt decreased, leading to the increase of the oxidation rate by strengthening the oxidative ability of adsorbed oxygen species.<sup>31</sup> A recent new calculation arrived at the same conclusion that  $\text{AuPt}_3$  has higher activity than Pt for the oxidation of  $\text{CO}_{\text{ads}}$  by the adsorbed ( $\text{O}_2$ )<sub>ads</sub> and/or  $\text{O}_{\text{ads}}$ .<sup>66</sup> Electrochemical results in Figure 4 also confirm that the reduction peak around 0 V for the adsorbed oxygen species at Pt sites shifts positively with the decrease of Pt content in the AuPt foam films. Therefore, we can effectively improve the catalytic activity of AuPt alloy by controlling its microstructure and surface composition via electrodeposition.

The long-term stability of the electrodeposited AuPt foam films for formic acid oxidation were investigated by chronoamperometric measurements in  $0.5\text{ M}$  formic acid +  $0.5\text{ M H}_2\text{SO}_4$ . As shown in Figure 5b, the current decayed more slowly and the steady current was much higher on the alloy foam films than on the commercial Etek-Pt/C (the dashed line).<sup>28</sup> These results show that AuPt alloy foams have better stability and the  $\text{Au}_{100}\text{Pt}_1$  foam catalyst is the most active and stable one among them in the formic acid oxidation reaction. However, accumulation of poison on the electrode surface may account for the gradual decrease in the oxidation current density of formic acid<sup>67</sup> in Figure 5b.

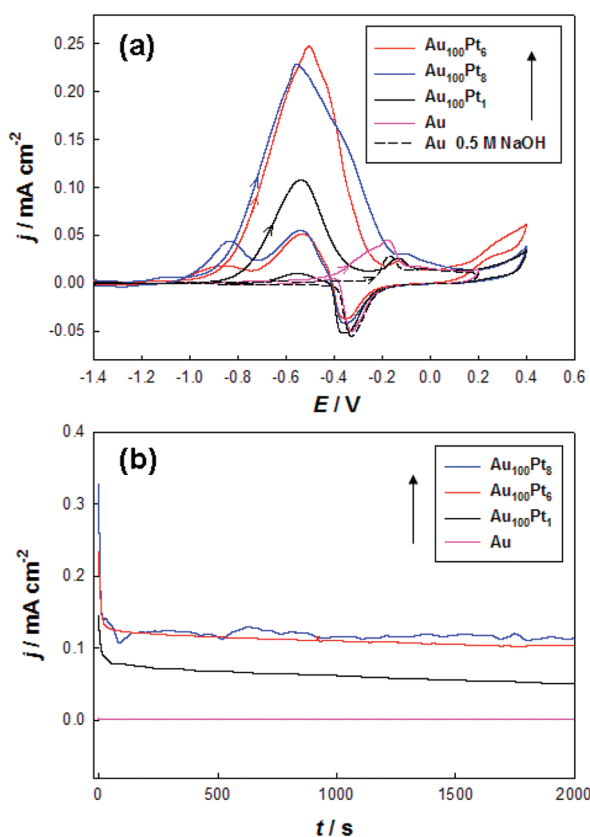


**Figure 7.** (a) CVs at  $20\text{ mV s}^{-1}$  and (b) chronoamperometric curves at  $-0.6\text{ V}$  in  $0.5\text{ M NaOH} + 0.5\text{ M CH}_3\text{OH}$  on the electrodeposited Au and AuPt foam films. The dashed line in panel a is the CV on the electrodeposited Au foam film in  $0.5\text{ M NaOH}$ .

To further prove that the poisonous intermediate formation reactions were inhibited on the AuPt foam films, we conducted stripping tests of the formed poison from the dissociation of formic acid at open circuit potential. As shown in Figure 6, there was a big sharp oxidation peak on the pure Pt electrode at  $0.09\text{ V}$  in the first positive potential sweep which is ascribed to the oxidation of  $\text{CO}_{\text{ads}}$  formed from the dissociative adsorption of formic acid.<sup>49</sup> However, this peak diminished and even vanished on the AuPt foams (Figure 6b–d), indicating there was less or no poisoning  $\text{CO}_{\text{ads}}$  formed from the dissociation of formic acid. It is possibly due to the fact that an absolutely small amount of poison, although formed, was not detectable with cyclic voltammetry.<sup>67</sup> A similar phenomenon has been reported on Pt modified Au electrocatalysts.<sup>68</sup>

**3.3. Electrocatalytic Oxidation of Methanol on the Alloy Foam Films.** The electrocatalytic activities of the resulting foam films of Au and AuPt for methanol oxidation were measured in an electrolyte containing  $0.5\text{ M NaOH}$  and  $0.5\text{ M CH}_3\text{OH}$ . It has been recognized that methanol oxidation on Au electrodes in alkaline solutions proceeds with different mechanisms depending on potentials:<sup>69,70</sup> at lower potentials, methanol was mainly oxidized to formate via an overall four-electron transfer reaction; whereas at higher potentials, methanol was oxidized to carbonate with a six-electron exchange. The oxidation peak of methanol on the AuPt foam films appeared at about  $-0.55\text{ V}$  (Figure 7a), negative to the initial oxidation potential of methanol on the Au foam film (about  $-0.5\text{ V}$ ). A similar phenomenon of Pt-modified nanoporous Au toward methanol oxidation has also been observed

previously.<sup>71</sup> The peak current densities on Au<sub>100</sub>Pt<sub>1</sub>, Au<sub>100</sub>Pt<sub>2</sub>, and Au<sub>100</sub>Pt<sub>8</sub> foam films are 0.107, 0.246, and 0.224 mA cm<sup>-2</sup>, respectively, indicating that further increase of Pt ratio larger than Au<sub>100</sub>Pt<sub>6</sub> is unnecessary to save the Pt resource. With an increase of Pt content in the AuPt foam, a shoulder peak appeared around -0.4 V in Figure 7a for Au<sub>100</sub>Pt<sub>6</sub>, which then broadened for Au<sub>100</sub>Pt<sub>8</sub>. We tentatively ascribe it to the contribution from Au which was enhanced by Pt, noting that this shoulder peak was observed for Au<sub>100</sub>Pt<sub>1</sub> and there was a broad oxidation peak on the Au foam film.

Figure 7b shows the current densities measured at -0.6 V (vs Hg/HgSO<sub>4</sub>). The Au<sub>100</sub>Pt<sub>8</sub> and Au<sub>100</sub>Pt<sub>6</sub> alloy foam films have comparable steady current density of about 0.11 mA cm<sup>-2</sup> at 2000 s, larger than that on the Au<sub>100</sub>Pt<sub>1</sub> (0.05 mA cm<sup>-2</sup>).

In addition to the electron effect involving d-band center shift as discussed above, ensemble effect should play an important role in the enhanced electrocatalytic activities for the oxidation of methanol on the AuPt alloy foam films. In contrary to the oxidation of formic acid, methanol oxidation needs an ensemble of minimum number of neighboring Pt atoms.<sup>20</sup> With the increase of Pt/Au ratio from Au<sub>100</sub>Pt<sub>1</sub> to Au<sub>100</sub>Pt<sub>6</sub>, the number of neighboring Pt atoms reached a better assembly to fulfill the requirements for the efficient electrocatalytic oxidation of methanol. Synergistic effect may also make some contribution for the electrooxidation of methanol on the AuPt foam films in the alkaline electrolyte.<sup>23</sup> The adsorbed poisoning CO<sub>ad</sub> on Pt sites and/or on Au atoms can be cleared up by the neighboring Au(OH)<sub>ad</sub> species formed by hydroxyl adsorption, preventing the catalyst from being poisoned.

## 4. CONCLUSIONS

In summary, AuPt alloy foam films have been successfully sculptured by coelectrodeposition using the simple hydrogen bubble dynamic template. The binding energy of Pt in the alloy decreased as a result of d-band shift. The AuPt alloy foam catalysts displayed superior electrocatalytic activity and long stability for the oxidation of formic acid. Under our experimental conditions, the foam film of Au<sub>100</sub>Pt<sub>1</sub> was the best among the AuPt alloy foams for the electrocatalytic oxidation of formic acid, where the dehydration pathway to form CO was completely suppressed mainly due to the assembly effect. Moreover, Au<sub>100</sub>Pt<sub>6</sub> and Au<sub>100</sub>Pt<sub>8</sub> foam films had comparable electrocatalytic performances for the oxidation of methanol, better than the Au<sub>100</sub>Pt<sub>1</sub> foam film. Ensemble effect, synergistic effect, and electronic effect may all make contributions for the improved activity toward the electrocatalytic oxidation of methanol.

## ■ ASSOCIATED CONTENT

**5 Supporting Information.** SEM images of Au foams under different conditions, CVs of the AuPt foam films in 0.5 M NaOH solution, data of d-spacings from the XRD, and data of comparison for electrocatalytic activity. This material is available free of charge via the Internet at <http://pubs.acs.org>.

## ■ AUTHOR INFORMATION

### Corresponding Author

\*Tel.: +86-731-88871533. Fax: +86-731-88872531. E-mail: lizelin@hunnu.edu.cn.

## ■ ACKNOWLEDGMENT

We are grateful for the financial support of this research though PhD Programs Foundation of the Education Ministry of China (Grant No. 20104306110003) and National Natural Science Foundation of China (Grant Nos. 20673103 and 21003045).

## ■ REFERENCES

- Teng, X. W.; Feygenson, M.; Wang, Q.; He, J. Q.; Du, W. X.; Frenkel, A. I.; Han, W. Q.; Aronson, M. *Nano Lett.* **2009**, *9*, 3177–3184.
- Luo, M. F.; Wang, C. C.; Hu, G. R.; Lin, W. R.; Ho, C. Y.; Lin, Y. C.; Hsu, Y. J. *J. Phys. Chem. C* **2009**, *113*, 21054–21062.
- Selvarani, G.; Selvaganes, S. V.; Krishnamurthy, S.; Kiruthika, G. V. M.; Sridhar, P.; Pitchumani, S.; Shukla, A. K. *J. Phys. Chem. C* **2009**, *113*, 7461–7468.
- Mark Ormerod, R.; Baddeley, C. J.; Lambert, R. M. *Surf. Sci. Lett.* **1991**, *259*, 709–713.
- Sachter, W. M. H.; Van Der Plank, P. *Surf. Sci.* **1969**, *18*, 62–79.
- Eley, D. D.; Moore, P. B. *Surf. Sci.* **1981**, *111*, 325–343.
- Nilius, N.; Wallis, T. M.; Ho, W. J. *Phys. Chem. B* **2004**, *108*, 14616–14619.
- Xu, J. B.; Zhao, T. S.; Liang, Z. X. *J. Phys. Chem. C* **2008**, *112*, 17362–17367.
- Liang, D.; Gao, J.; Wang, J. H.; Chen, P.; Wei, Y. F.; Hou, Z. Y. *Catal. Commun.* **2011**, *12*, 1059–1062.
- Suo, Y. G.; Hsing, I. M. *Electrochim. Acta* **2011**, *56*, 2174–2183.
- Jia, J. B.; Cao, L. Y.; Wang, Z. H. *Langmuir* **2008**, *24*, 5932–5936.
- Yen, C. H.; Shimizu, K.; Lin, Y. Y.; Bailey, F.; Cheng, I. F.; Wai, C. M. *Energy Fuels* **2007**, *21*, 2268–2271.
- Lee, Y. W.; Kim, M.; Kim, Y.; Kang, S. W.; Lee, J. W.; Han, S. W. *J. Phys. Chem. C* **2010**, *114*, 7689–7693.
- Ge, X. B.; Yan, X. L.; Wang, R. Y.; Tian, F.; Ding, Y. *J. Phys. Chem. C* **2009**, *113*, 7379–7384.
- Yang, L. X.; Yang, W. Y.; Cai, Q. Y. *J. Phys. Chem. C* **2007**, *111*, 16613–16617.
- Hernández-Fernández, P.; Rojas, S.; Ocón, P.; Gómez de la Fuente, J. L.; San Fabián, J.; Sanza, J.; Peña, M. A.; García-García, F. J.; Terreros, P.; Fierro, J. L. G. *J. Phys. Chem. C* **2007**, *111*, 2913–2923.
- Guo, S. J.; Wang, L.; Dong, S. J.; Wang, E. K. *J. Phys. Chem. C* **2008**, *112*, 13510–13515.
- Lou, Y. B.; Maye, M. M.; Han, L.; Luo, J.; Zhong, C. *J. Chem. Commun.* **2001**, 473–474.
- Safavi, A.; Farjami, F. *Biosens. Bioelectron.* **2011**, *26*, 2547–2552.
- Du, B. C.; Tong, Y. Y. *J. Phys. Chem. B* **2005**, *109*, 17775–17780.
- Hu, Y. J.; Zhang, H.; Wu, P.; Zhang, H.; Zhou, B.; Cai, C. X. *Phys. Chem. Chem. Phys.* **2011**, *13*, 4083–4094.
- Shin, T. Y.; Yoo, S. H.; Park, S. *Chem. Mater.* **2008**, *20*, 5682–5686.
- Luo, J.; Njoki, P. N.; Lin, Y.; Mott, D.; Wang, L. Y.; Zhong, C. J. *Langmuir* **2006**, *22*, 2892–2898.
- Tang, W.; Jayaraman, S.; Jaramillo, T. F.; Stucky, G. D.; McFarland, E. W. *J. Phys. Chem. C* **2009**, *113*, 5014–5024.
- Min, M.; Kim, C.; Lee, H. *J. Mol. Catal. A: Chem.* **2010**, *333*, 6–10.
- Zhang, Y.; Huang, Q. H.; Zou, Z. Q.; Yang, J. F.; Vogel, W.; Yang, H. *J. Phys. Chem. C* **2010**, *114*, 6860–6868.
- Mott, D.; Luo, J.; Njoki, P. N.; Lin, Y.; Wang, L. Y.; Zhong, C. J. *Catal. Today* **2007**, *122*, 378–385.
- Zhang, S.; Shao, Y. Y.; Liao, H. G.; Liu, J.; Aksay, I. A.; Yin, G. P.; Lin, Y. H. *Chem. Mater.* **2011**, *23*, 1079–1081.
- Lin, Z. H.; Shih, Z. Y.; Tsai, H. Y.; Chang, H. T. *Green Chem.* **2011**, *13*, 1029–1035.
- Ge, X. B.; Wang, R. Y.; Cui, S. Z.; Tian, F.; Xu, L. Q.; Ding, Y. *Electrochim. Commun.* **2008**, *10*, 1494–1497.
- Ruban, A.; Hammer, B.; Stoltze, P.; Skriver, H. L.; Nørskov, J. K. *J. Mol. Catal. A: Chem.* **1997**, *115*, 421–429.

- (32) Paxton, W. F.; Kistler, K. C.; Olmeda, C. C.; Sen, A.; St Angelo, S. K.; Cao, Y. Y.; Mallouk, T. E.; Lammert, P. E.; Crespi, V. H. *J. Am. Chem. Soc.* **2004**, *126*, 13424–13431.
- (33) Teng, X. W.; Han, W. Q.; Wang, Q.; Li, L.; Frenkel, A. I.; Yang, J. C. *J. Phys. Chem. C* **2008**, *112*, 14696–14701.
- (34) Yang, S. C.; Hong, F.; Wang, L. Q.; Guo, S. W.; Song, X. P.; Ding, B. J.; Yang, Z. M. *J. Phys. Chem. C* **2010**, *114*, 203–207.
- (35) Tong, X. L.; Zhao, G. H.; Liu, M. C.; Cao, T. C.; Liu, L.; Li, P. Q. *J. Phys. Chem. C* **2009**, *113*, 13787–13792.
- (36) Shchukin, D. G.; Caruso, R. A. *Chem. Mater.* **2004**, *16*, 2287–2292.
- (37) Liu, F.; Yan, Q. F.; Zhou, W. J.; Zhao, X. S.; Lee, J. Y. *Chem. Mater.* **2006**, *18*, 4328–4335.
- (38) He, H.; Cai, W. P.; Lin, Y. X.; Dai, Z. F. *Langmuir* **2011**, *27*, 1551–1555.
- (39) Lu, L.; Eychmüller, A. *Acc. Chem. Res.* **2008**, *41*, 244–253.
- (40) Jin, H. J.; Wang, X. L.; Parida, S.; Wang, K.; Seo, M.; Weissmuller, J. *Nano Lett.* **2010**, *10*, 187–194.
- (41) Zhang, J. T.; Liu, P. P.; Ma, H. Y.; Ding, Y. *J. Phys. Chem. C* **2007**, *111*, 10382–10388.
- (42) Liu, W. B.; Zhang, S. C.; Li, N.; Zheng, J. W.; Xing, Y. L. *Microporous Mesoporous Mater.* **2011**, *138*, 1–7.
- (43) Plowman, B. J.; Mullane, A. P. O.; Selvakannan, P. R.; Bhargava, S. K. *Chem. Commun.* **2010**, *46*, 9182–9184.
- (44) Cherevko, S.; Chung, C. H. *Electrochem. Commun.* **2011**, *13*, 16–19.
- (45) Cherevko, S.; Chung, C. H. *Electrochim. Acta* **2010**, *55*, 6383–6390.
- (46) Shin, H. C.; Dong, J.; Liu, M. L. *Adv. Mater.* **2003**, *15*, 1610–1614.
- (47) Shin, H. C.; Liu, M. L. *Chem. Mater.* **2004**, *16*, 5460–5464.
- (48) Shin, H. C.; Liu, M. L. *Adv. Funct. Mater.* **2005**, *15*, 582–586.
- (49) Clavilier, J.; Sun, S. G. *J. Electroanal. Chem.* **1986**, *199*, 471–480.
- (50) Crist, B. V. *Handbook of Monochromatic XPS Spectra*; Wiley: Chichester/New York, 2000.
- (51) Bagus, P. S.; Nelin, C. J.; Ilton, E. S.; Baron, M.; Abbott, H.; Primorac, E.; Kuhlenbeck, H.; Shaikhutdinov, S.; Freund, H.-J. *Chem. Phys. Lett.* **2010**, *487*, 237–240.
- (52) Bagus, P. S.; Eugene, S. I. *Phys. Rev. B* **2006**, *73*, 155110.
- (53) Tada, H.; Suzuki, F.; Ito, S.; Akita, T.; Tanaka, K.; Kawahara, T.; Kobayashi, H. *J. Phys. Chem. B* **2002**, *106*, 8714–8720.
- (54) Park, K. W.; Choi, J. H.; Sung, Y. E. *J. Phys. Chem. B* **2003**, *107*, 5851–5856.
- (55) Xiao, F.; Mo, Z. R.; Zhao, F. Q.; Zeng, B. Z. *Electrochem. Commun.* **2008**, *10*, 1740–1743.
- (56) Deng, L.; Hu, W. Y.; Deng, H. Q.; Xiao, S. F. *J. Phys. Chem. C* **2010**, *114*, 11026–11032.
- (57) Xiao, S.; Hu, W.; Luo, W.; Wu, Y.; Li, X.; Deng, H. *Eur. Phys. J. B* **2007**, *54*, 479–484.
- (58) Liz-Marzan, L. M.; Philipse, A. P. *J. Phys. Chem.* **1995**, *99*, 15120–15128.
- (59) Wanjala, B. N.; Luo, J.; Fang, B.; Mott, D.; Zhong, C. J. *J. Mater. Chem.* **2011**, *21*, 4012–4020.
- (60) Lang, H. F.; Maldonado, S.; Stevenson, K. J.; Chandler, B. D. *J. Am. Chem. Soc.* **2004**, *126*, 12949–12956.
- (61) Chandler, B. D.; Schabel, A. B.; Pignolet, L. H. *J. Phys. Chem. B* **2000**, *105*, 149–155.
- (62) Burke, L. D.; Mullane, A. P. O.; Vincent, E. L.; Mooney, M. B. *J. Solid State Electrochem.* **2001**, *5*, 319–327.
- (63) Capon, A.; Parson, R. *J. Electroanal. Chem.* **1973**, *44*, 1–7.
- (64) Capon, A.; Parsons, R. *J. Electroanal. Chem.* **1973**, *45*, 205–231.
- (65) Neurock, M.; Janik, M.; Wieckowski, A. *Faraday Discuss.* **2009**, *140*, 363–378.
- (66) García-Motaw, M.; López, N. *Phys. Chem. Chem. Phys.* **2011**, *13*, 5790–5797.
- (67) Kim, S.; Jung, C. H.; Kim, J.; Rhee, C. K.; Choi, S. M.; Lim, T. H. *Langmuir* **2010**, *26*, 4497–4505.
- (68) Kristian, N.; Yu, Y. L.; Gunawan, P.; Xu, R.; Deng, W. Q.; Liu, X. W.; Wang, X. *Electrochim. Acta* **2009**, *54*, 4916–4924.
- (69) Borkowska, Z.; Tymosiak-Zielinska, A.; Nowakowski, R. *Electrochim. Acta* **2004**, *49*, 2613–2621.
- (70) Borkowska, Z.; Tymosiak-Zielinska, A.; Shul, G. *Electrochim. Acta* **2004**, *49*, 1209–1220.
- (71) Wang, X. G.; Frenzel, J.; Wang, W. M.; Ji, H.; Qi, Z.; Zhang, Z. H.; Eggeler, G. *J. Phys. Chem. C* **2011**, *115*, 4456–4465.